Timing Jitter in Dispersion-Managed Soliton Systems With Distributed, Lumped, and Hybrid Amplification

Ekaterina Poutrina, *Student Member, IEEE*, and Govind P. Agrawal, *Fellow, IEEE*

***Abstract*—We analyze the role of distributed amplification in controlling timing jitter in dispersion-managed soliton systems and discuss, using analytical and numerical techniques, how timing jitter is reduced by up to a factor of two when lumped amplification is replaced by complete or partial distributed amplification. We derive an analytical expression for the timing jitter at any position within the fiber link in the case of ideal distributed amplification for which losses are exactly compensated by gain at every point. We show that the timing jitter is well approximated by this formula in the case of erbium-based amplification. We derive a similar expression for the timing jitter for lumped amplifiers and compare it with the case of distributed amplification. We find that with erbium-based distributed amplification, timing jitter depends on the density of dopants and is smaller for lower densities. In the case of hybrid Raman amplification, the transmission distance of a 40-Gb/s system can be increased by up to 30% depending on the amount of Raman gain. Finally, we show that timing jitter decreases for stronger maps at a given bit rate (constant minimum pulsewidth).**

***Index Terms*—Dispersion management, jitter, nonlinear optics, optical fiber communication, optical solitons.**

I. Introduction

GORDON–HAUS timing jitter, arising from the presence of amplified spontaneous emission (ASE) in modern fiber links, is one of the major limiting factors for long-haul optical communication systems, especially at high bit rates exceeding 10 Gb/s [1]–[9]. A general approach for calculating timing jitter in dispersion-managed (DM) systems was developed by Grigoryan *et al.* in 1999 [3]. In the past, attention was mostly paid to estimating timing jitter in lightwave systems with lumped amplifiers placed periodically along the DM link [4]–[6]. Although the effect of distributed amplification on timing jitter has been studied for uniform-dispersion fibers [7], [8], the combination of distributed amplification and dispersion management has not yet been investigated.

We use the approach developed in [3] to compare the ASE-induced timing jitter in DM systems for the cases of lumped, distributed, and hybrid Raman amplification. In Section II, we extend the theory of [3] to the case of distributed amplification. In Section III, we derive an analytic expression for the timing jitter at any position within the fiber link in the case of ideal distributed amplification for which losses are compensated by gain perfectly at every point. We also derive an analytical expression for the timing jitter induced by lumped amplifiers and compare the two cases. In Section IV, we investigate timing jitter in DM systems for the case of erbium-based distributed amplification, realized when the transmission fiber itself is lightly doped with erbium ions. We show that timing jitter can be reduced by about 40% with proper system design and is quite close to the ideal case. In Section V, we consider timing jitter in DM soliton systems making use of Raman amplification. We show that considerable jitter reduction occurs when bidirectional, backward, or even partial Raman amplification is employed. We also investigate timing jitter dependence on other system parameters such as the bit rate and the map strength.

Manuscript received May 15, 2001; revised January 28, 2002. This work was supported in part by the National Science Foundation under Grant ECS-9903580 and Grant DMS-0073923.

The authors are with the Institute of Optics, University of Rochester, Rochester, NY 14627 USA.

Publisher Item Identifier S 0733-8724(02)03198-5.

II. General Formalism

We give in this section a short description of the moment method for calculating timing jitter [3]. Optical pulse propagation in any lightwave system is governed by the nonlinear Schrödinger (NLS) equation [9]

$$\frac{\partial u}{\partial z} = -i\frac{\beta_2}{2}\frac{\partial^2 u}{\partial t^2} + i\gamma_0|u^2|u + \frac{1}{2}(g-\alpha)u + f_n(z,t) \quad (1)$$

where $g(z)$ and $\alpha(z)$ are, respectively, local power gain and loss inside the fiber, γ_0 is the nonlinear coefficient, β_2 is the second-order dispersion parameter, and $f_n(z,t)$ represents the contribution of noise (distributed or lumped) along the fiber length. The ASE noise contribution vanishes on average, i.e., $\langle f_n(z,t)\rangle = 0$, but has a correlation function of the form [9], [10]

$$\langle f_n(z,t) f_n^*(z',t')\rangle = g(z) n_{\rm sp}(z) h\nu_0 \delta(z-z')\delta(t-t') \quad (2)$$

where $n_{\rm sp}(z)$ is the spontaneous emission factor, $h\nu_0$ is the photon energy at the central frequency ν_0, and δ represents Dirac's delta function. Both $n_{\rm sp}(z)$ and $g(z)$ are nonzero only within the amplifier in the case of lumped amplification, but vary with z continuously in the case of distributed amplification.

In the moment method [11], the central position t_p and the central frequency Ω of an optical pulse are defined as

$$t_p(z) = \int_{-\infty}^{\infty} t|u|^2\,dt \Big/ E \quad (3a)$$

$$\Omega(z) = \int_{-\infty}^{\infty} (u_t^* u - u_t u^*)\,dt \Big/ 2iE \quad (3b)$$

where u_t stands for the time derivative of u and

$$E(z) = \int_{-\infty}^{\infty} |u(z,t)|^2\,dt \quad (4)$$

is the energy of the pulse. We introduce a new variable v in (1)–(4) using the definition $u = \sqrt{G}v$, where G represents the cumulative net gain from 0 to z and is given by

$$G(z) \equiv \exp\left(\int_0^z [g(z') - \alpha(z')]\, dz'\right). \tag{5}$$

In order to calculate the timing jitter, it is necessary to know how t_p and Ω evolve with z. Following [3], (3) for t_p and Ω are differentiated with respect to z and (1) is used to eliminate $\partial u/\partial z$. One can integrate the resulting differential equations and introduce the random time shift $\delta t_p \equiv t_p - \langle t_p \rangle$, which is found to vary with z as

$$\delta t_p(z) = \mathcal{F}(z) + \mathcal{S}(z) \tag{6}$$

where $\mathcal{F}$ and $\mathcal{S}$ represent the contributions to δt_p from frequency and position fluctuations, occurring due to ASE noise along the fiber link. Their explicit expressions are

$$\mathcal{F}(z) = \int_0^z \beta_2(z')\delta\Omega(z')\, dz' \tag{7}$$

$$\mathcal{S}(z) = i\int_0^z \left\{\frac{\sqrt{G}}{E}\int_{-\infty}^{\infty}(t - t_p) \cdot[q f_n^* \exp(-i\Omega t) - q^* f_n \exp(i\Omega t)]\, dt\right\} dz' \tag{8}$$

where $\delta\Omega$ is defined as

$$\delta\Omega(z) \equiv -\int_0^z \left\{\frac{\sqrt{G}}{E}\int_{-\infty}^{\infty} \cdot[q_t^* f_n \exp(i\Omega t) + q_t f_n^* \exp(-i\Omega t)]\, dt\right\} dz'. \tag{9}$$

In (7)–(9), q is defined as $q = v\exp(i\Omega t)$. As discussed in [3], q and E in (8) and (9) correspond to the deterministic solution of (1), obtained after setting $f_n = 0$. Linearized equations (6)–(9) are used to calculate the timing jitter σ defined as $\sigma^2 = \langle (\delta t_p)^2 \rangle$ and given by

$$\sigma^2 = \langle \mathcal{F}^2 \rangle + 2\langle \mathcal{F}\mathcal{S} \rangle + \langle \mathcal{S}^2 \rangle. \tag{10}$$

Following [3], expressions for $\langle \mathcal{F}^2 \rangle$, $\langle 2\mathcal{F}\mathcal{S} \rangle$, and $\langle \mathcal{S}^2 \rangle$ terms, valid for arbitrary pulse shape, are obtained. We apply those expressions to a chirped Gaussian pulse of the form

$$u(z, t) = u_0 \exp\left(-\frac{(1 + iC)(t - t_p)^2}{2T^2} - i\Omega(t - t_p) + i\phi\right) \tag{11}$$

where C is chirp, T is the pulsewidth at $1/e$ point, u_0 is the peak amplitude of the pulse, and ϕ is the phase. We then obtain the following expressions:

$$\langle \mathcal{F}^2 \rangle = \frac{2h\nu_0}{E_0}\int_0^z \beta_2(z_1)\, dz_1 \int_0^{z_1} \beta_2(z_2)\, dz_2 \cdot \int_0^{z_2} g(z')n_{\rm sp}(z')\frac{1 + C^2(z')}{G(z')T^2(z')}\, dz' \tag{12a}$$

$$\langle \mathcal{F}\mathcal{S} \rangle = \frac{h\nu_0}{E_0}\int_0^z \beta_2(z_1)\, dz_1 \int_0^{z_1} g(z')n_{\rm sp}(z') \cdot G^{-1}(z')C(z')\, dz' \tag{12b}$$

$$\langle \mathcal{S}^2 \rangle = \frac{h\nu_0}{E_0}\int_0^z g(z')n_{\rm sp}(z')G^{-1}(z')T^2(z')\, dz' \tag{12c}$$

where $E_0 \equiv E(0)$ is the input energy of the pulse. Equations (10) and (12) provide semi-analytical expressions for the timing jitter. They can be used for any amplification scheme, whether lumped, distributed, or hybrid. The only assumption made is that we use a chirped Gaussian shape for pulses propagating inside a DM system. Analyses based on the variational and Hermite–Gauss-expansion methods have shown [12], [13] that numerically calculated pulse shapes are close to Gaussian (except in the pulse wings). In the next section, we justify this approximation by comparing timing jitter calculated using the actual pulse shape (taken from a NLS-based propagation code) and the pulse shape given by (11).

III. Analytical Treatment

In this section, we use (12) to calculate variances and cross correlation of $\mathcal{F}$ and $\mathcal{S}$ for a DM soliton communication system and calculate timing jitter for lumped and distributed amplification scheme. We focus on the case of ideal distributed amplification first. We consider a DM system in which each map period L_m consists of two fiber sections with dispersion parameters β_{21} and β_{22}, respectively, and the local gain $g(z) \equiv \alpha$ at every point, so that $G(z) = 1$ in (12). We assume for simplicity that both fiber sections have the same value of losses α. The results can be generalized later to the case of an arbitrary loss profile. The variables $G(z)$, $g(z)$, and $n_{\rm sp}(z)$ are now constants in (12). Using the variational equation for the pulsewidth [9] in (12b), we can express the variance of $\mathcal{S}$ in terms of cross correlation of $\mathcal{F}$ and $\mathcal{S}$ as

$$\langle \mathcal{S}^2 \rangle = 2\langle \mathcal{F}\mathcal{S} \rangle + Q_d T_0^2 z/L_m \tag{13}$$

where

$$Q_d \equiv h\nu_0 n_{\rm sp} g L_m/E_0 \tag{14}$$

is a dimensionless parameter.

To calculate the variance of $\mathcal{F}$ and cross correlation of $\mathcal{F}$ and $\mathcal{S}$, we need to calculate in (12) the integrals like

$$I_1(z) \equiv \int_0^z \frac{1 + C^2(z)}{T^2(z)}\, dz, \quad I_2(z) \equiv \int_0^z C(z)\, dz. \tag{15}$$

Performing the first integral numerically, we find that I_1 grows with z almost linearly (with an accuracy of about 0.01%) as $I_1(z) \approx (1 + C_0^2)/T_0^2$, where C_0 and T_0 are the input values of chirp and pulsewidth, respectively. This result has a physical basis since the ratio $\sqrt{1 + C^2(z)}/T(z)$ represents the spectral width of a chirped pulse. The spectral width remains constant for a linear system and does not change much if the nonlinear length of the system is much larger than the local dispersion length. Even numerical solutions of the nonlinear variational equations show that the ratio $\sqrt{1 + C^2(z)}/T(z)$ oscillates around its input value within each map period with a negligible amplitude. To estimate the second integral in (14), we

approximate $C(z)$ by a linear function of z in each fiber section and make use of the fact that, for ideal loss compensation ($g = \alpha$), the chirp-free point is located in the middle of each fiber section [12].

Using (13) in (12a), we perform the remaining two integrations for calculating $\langle \mathcal{F}^2 \rangle$ using a geometrical approach. In short, noting that $\beta_2(z_2)I_1(z_2)$ is a piecewise continuous function, we carry out the integration over z_2. We then repeat the same process for integrating over z_1 and complete the integration in (12b) and (12c). Using the notation $z = mL_m + x$, where m is the number of complete map periods up to the distance z and x is a fractional distance in the next map period ($0 \le x \le L_m$), the final result for timing jitter is given as

$$\begin{aligned}\sigma_d^2(m,x) &= Q_d \frac{1+C_0^2}{T_0^2} \\ &\cdot [b_0^2 m(m-1)(2m-1)/6 + b_0 b_1 m(m-1)/2 + \Delta_0 m/3 \\ &\quad + b(x) b_0 m(m-1) + b^2(x) m + b(x) b_1 m + \Delta(x)/3] \\ &+ Q_d 4C_0[\varepsilon_0 m + \varepsilon(x)] + Q_d T_0^2 [m + x/L_m] \end{aligned} \tag{16}$$

where $b(x)$ is the dispersion accumulated over a distance x:

$$b(x) \equiv \int_0^x \beta_2(x')\, dx' \tag{17}$$

so that $b_0 \equiv b(L_m) = b_{21} l_1 + b_{22} l_2 = \overline{\beta}_2 L_m$, $\overline{\beta}_2$ being the average dispersion of the map. Further, $b_1 \equiv b_0 + (\beta_{22} - \overline{\beta}_2) l_2$, and the functions $\Delta(x)$ and $\varepsilon(x)$ are defined as

$$\Delta(x) \equiv \begin{cases} x b^2(x)/L_m, & \text{if } 0 \le x \le l_1 \\ [l_1 b(x)[b(x) + \beta_{22}(x - l_1)] & \\ \quad + \beta_{22}^2 (x-l_1)^2 x]/L_m, & \text{if } l_1 \le x \le L_m \end{cases} \tag{18}$$

$$\varepsilon(x) \equiv \begin{cases} \beta_{21}(x^2/2 - x^3/3)/L_m, & \text{if } 0 \le x \le l_1 \\ \dfrac{1}{L_m}\left[\dfrac{\beta_{21} l_1^2}{6} - \beta_{22}\left(\dfrac{(x-l_1)^2}{2} - \dfrac{(x-l_1)^3}{3}\right)\right], & \\ \qquad \text{if } l_1 \le x \le L_m \end{cases} \tag{19}$$

where $\Delta_0 \equiv \Delta(L_m)$, $\varepsilon_0 \equiv \varepsilon(L_m)$ in (16).

Before discussing this analytic result, we derive a similar formula for the lumped amplification case, for which both $n_{\rm sp}(z)$ and $g(z)$ are nonzero only within each amplifier whose length is quite short (~10 m). Using $G_l = \exp(\alpha L_A)$ for the amplifier gain, where L_A is the amplifier spacing, the integrals in (12) can be performed analytically as

$$\frac{h\nu_0}{E_0} \int_0^{z_2} g(z_2') n_{\rm sp}(z_2') \frac{1 + C(z_2')^2}{G(z_2') T(z_2')^2}\, dz_2' = Q_l \frac{1+C_0^2}{T_0^2} N_l(z_2) \tag{20a}$$

$$\frac{h\nu_0}{E_0} \int_0^{z_1} g(z_1') n_{\rm sp}(z_1') G^{-1}(z_1) C(z_1)\, dz_1' = Q_l C_0 N_l(z_1) \tag{20b}$$

$$\frac{h\nu_0}{E_0} \int_0^{z} g(z') n_{\rm sp}(z') G^{-1}(z') T_0^2(z')\, dz' = Q_l T_0^2 N_l(z) \tag{20c}$$

where $N_l(z_i)$ is a staircase function representing the number of amplifiers up to the coordinate z_i, and

$$Q_l \equiv h\nu_0 n_{\rm sp}(G_l - 1)/E_0. \tag{21}$$

Using (20), we complete the integrations in (12), employing the same geometrical approach described earlier. The final result for the variance of timing jitter at a distance $z = nL_A + x$ in system with an arbitrary dispersion map within each amplification period is given as

$$\begin{aligned}\sigma_l^2(n,x) = Q_l \frac{1+C_0^2}{T_0^2} &[b_0^2 n(n-1)(2n-1)/6 \\ &+ b(x) b_0 n(n-1) + b^2(x) n] \\ &+ Q_l C_0 [b_0 n(n-1) + 2b(x) n] + Q_l T_0^2 n \end{aligned} \tag{22}$$

where n is the number of amplifiers up to the distance z and x is the fractional distance in the next amplification period ($0 \le x \le L_A$). We keep different notations for amplification period L_A and map period L_m since (22) applies to the case of dense DM in which each amplification period contains several map periods.

From (16) and (22), we note that the largest contribution to timing jitter comes from the first term resulting from frequency fluctuations and increasing with distance as z^3. If we use (9), the variance of frequency fluctuations $\langle \delta\Omega^2 \rangle$, accumulated within one map period (or amplification period in the case of lumped amplifiers) is given by

$$\langle \delta\Omega^2 \rangle_{d,l} = Q_{d,l} \frac{1+C_0^2}{T_0^2} \tag{23}$$

where the subscripts d and l stand for distributed and lumped amplification, respectively. In (16) and (22), the term in the first square brackets represents the variance $\langle \mathcal{F}^2 \rangle$. For constant-dispersion fibers ($\beta_{21} = \beta_{22} \equiv \beta_2$) and for lumped amplification, $\langle \mathcal{F}^2 \rangle$ term with $x = 0$ converts to the standard Gordon–Haus formula [1], [2] $\langle \mathcal{F}^2 \rangle = \langle \delta\Omega^2 \rangle_l \beta_2^2 L_A^2 \sum_{i=1}^{n} (n-i)^2$. We have also verified that, for constant dispersion, $\langle \delta\Omega^2 \rangle_l$ reduces to the equivalent expression in [1], [2] when a hyperbolic secant pulse shape is used instead of a Gaussian shape in (11).

We now focus on the effect of distributed amplification on timing jitter. Consider first the timing jitter at the end of a map period by setting $x = 0$. Several differences are apparent from (16) and (22). In the case of lumped amplification, the $\langle \mathcal{F}^2 \rangle$ term depends only on the average dispersion irrespective of the actual map configuration, while this is not the case for ideal distributed amplification. The $\langle \mathcal{FS} \rangle$ term grows as z^2 for lumped amplification, but only linearly with z in (16), indicating that cross correlation is less important in the case of distributed amplification. For lumped amplification, the variance $\langle \mathcal{S}^2 \rangle$, representing direct temporal shift of a soliton by ASE, does not depend on dispersion, but this is not so for distributed amplification, as seen from (13). This is the consequence of the fact that such position fluctuations happen only when noise is added. For lumped amplification, noise is not added outside amplifiers, while noise is added all along the fiber length in the case of distributed amplification.

Consider now the timing jitter inside a map period so that $x \neq 0$. As seen from (16) and (22), the x-dependent terms provide additional contribution to timing jitter within each map period, which depends on the accumulated dispersion $b(x)$ over the fractional distance x within each map period L_m (or the amplification period L_A). Since $b(x)$ is periodic, we expect timing jitter to exhibit oscillatory behavior. As seen from (16) and (22), the amplitude of such oscillations grows as z^2 with distance, while the first term in (16) and in (22) grows as z^3. This means that jitter never oscillates down to zero as z increases and the relative contribution of the oscillating terms to the total timing jitter decreases as $1/z$. For long distances such that $L \gg L_m$, taking the limit $m \gg 1$ and $n \gg 1$ in x-dependent terms in (16) and (22), we note that this additional contribution is positive or negative depending on the sign of the product $b(x)b_0$. For example, for the system with an even number of fiber sections within the map period, this contribution is negative if the sign of β_{21} is opposite to the sign of average dispersion $\overline{\beta}_2$.

An important question is how much timing jitter can be reduced by using distributed amplification. To answer this question, we consider a long-haul light-wave system such that the number of map periods L_m (or amplifiers in the case of lumped amplification) is very large. Taking the limit $m \gg 1$ and $n \gg 1$ in (16) and (22), the timing jitter is reduced for distributed amplification by the factor

$$f_r \equiv \frac{\sigma_d^2}{\sigma_l^2} \approx \frac{\langle \delta\Omega^2 \rangle_d}{\langle \delta\Omega^2 \rangle_l} = \frac{\alpha L_A}{(G_l - 1)} \frac{n_{\rm sp}^d}{n_{\rm sp}^l} \frac{E_0^l}{E_0^d} \frac{[(1 + C_0^2)/T_0^2]_d}{[(1 + C_0^2)/T_0^2]_l}. \tag{24}$$

In most cases of practical interest, $[(1 + C_0^2)/T_0^2]_l \approx [(1 + C_0^2)/T_0^2]_d$ when the system is designed to have the same value of the minimum pulsewidth. The energy ratio $E_0^l/E_0^d > 1$ under such conditions, increasing f_r. However, this increase, being of the order of $G_l \ln G_l/(G_l - 1)$, does not overcome the reduction in timing jitter due to the ratio $aL_A/(G_l - 1)$. The net result is that timing jitter can be reduced by using distributed amplification.

Fig. 1 shows timing jitter for lumped and distributed amplification schemes calculated at the end of each amplifier (each map period in the distributed case) using (16) and (22) based on the Gaussian shape ansatz (solid curves). To estimate the error introduced by this ansatz, circles show the results when the exact pulse shape obtained by solving the NLS equation is used in (10). In the lumped case, we consider a dense DM system with an amplifier spacing of 80 km and assume eight map periods within one amplifier period. Each map period has 5 km of fiber with $\beta_{21} = 3.9$ ps^2/km and 5 km of fiber with $\beta_{22} = -4.1$ ps^2/km, resulting in the average dispersion of -0.1 ps^2/km. Losses in each fiber section are 0.2 dB/km, and the value of nonlinearity is $\gamma_0 = 2.5\,\mathrm{W}^{-1}\mathrm{km}^{-1}$. The input pulse parameters (width T, chirp C, and energy E_0) are obtained by solving the variational equations numerically [9]. The minimum value $T_{\min}$ of pulsewidth is kept fixed at 3.11 ps [full-width at half-maximum (FWHM) 5.18 ps] in all cases to ensure a 40-Gb/s bit rate. For lumped amplification, the input parameters

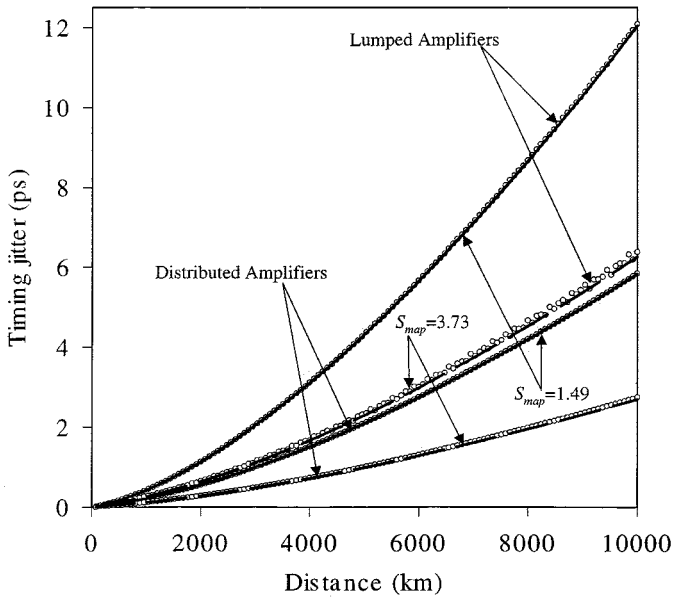

Fig. 1. Comparison of timing jitter as a function of transmission distance for lumped and ideal distributed amplification schemes for dispersion maps with $S_{\rm map} = 1.49$ (solid lines) and $S_{\rm map} = 3.73$ (dashed lines). Circles represent results obtained using the numerical pulse shape.

are $T_0 = 4.94$ ps, $C = -1.2$, $E_0 = 0.22$ pJ, while for ideal distributed amplification $T_0 = 4.47$ ps, $C = -1.0$, and $E_0 = 0.0597$ pJ. The map strength of this system, defined as

$$S_{\rm map} = \frac{(\beta_{21} - \overline{\beta}_2)\, l_1 - (\beta_{22-} - \overline{\beta}_2)\, l_2}{T_{\rm FWHM}^2} \tag{25}$$

where $T_{\rm FWHM} \approx 1.665 T_{\min}$ is the FWHM of the pulse at the minimum pulsewidth point, equal to $S_{\rm map} \approx 1.49$.

Since the deviation of pulse shape from Gaussian ansatz increases with map strength, we consider a similar system with a map strength of $S_{\rm map} \approx 3.73$. To increase the map strength we keep same geometry but increase dispersion values in both fiber sections to $\beta_{21} = 9.9$ ps^2/km, $\beta_{22} = -10.1$ ps^2/km. The input parameters in this case are $T_0 = 8.61$ ps, $C = -2.31$, $E_0 = 0.729$ pJ, for lumped amplification, and $T_0 = 8.29$ ps, $C = -2.31$, $E_0 = 0.270$ pJ, in the ideal distributed amplification case. In all cases we use $n_{\rm sp} = 1.5$ for lumped amplifiers (corresponds to a noise figure of 4.8 dB) and $n_{\rm sp} = 1$ for ideal distributed amplification.

Several conclusions can be drawn from Fig. 1. Timing jitter increases with transmission distance L as L^3 in all cases, as expected for the Gordon–Haus jitter. However, it is smaller by about a factor of 2 when distributed amplification is used. The approximations made in deriving (16) and (22) lead to the 0.02% error in comparison with the result of (12) and are not noticeable at the scale of Fig. 1. The curves calculated using the exact pulse shape (obtained by solving the NLS equation) show that the error in timing jitter values when using a Gaussian pulse shape is less than 2% and nearly vanishes for smaller values of $S_{\rm map}$.

To see how well (24) for the reduction factor works, we compare its predictions with the results shown in Fig. 1. We find that the error in the reduction factor given by (24), in comparison with the similar factor calculated using full analytical theory

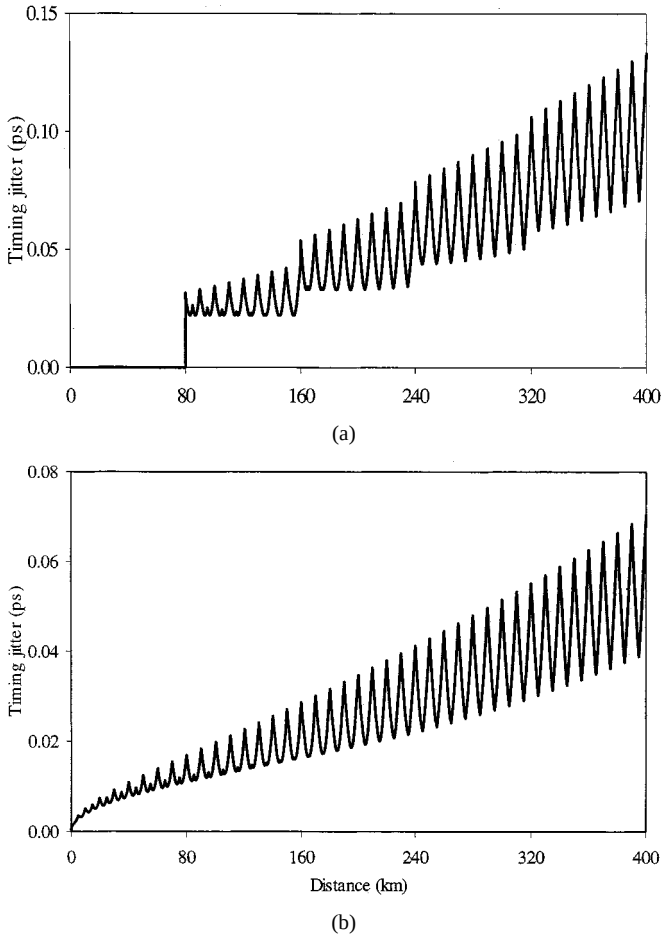

Fig. 2. Timing jitter variations within each map period for lumped and distributed amplification for the map with $S_{\rm map} = 1.49$.

[(16) and (22)] reduces to less than 10% after about seven amplification periods. Moreover, at distances larger than 14 amplification periods, the error becomes less than 5%. We have also verified that these error values do not change much with the map strength.

Fig. 2 shows how timing jitter oscillates within each map period for lumped and distributed amplification schemes. In the lumped case [Fig. 2(a)], no jitter occurs until the first amplifier is encountered at a distance of 80 km. Since in the map considered, the sign of β_{21} is opposite to the sign of average dispersion, jitter is reduced within each map period in comparison with its values in the ends of the periods. The value in the end of each period increases with distance as L^3. For long distances such that $L \gg L_m$, eventually the oscillations in timing jitter within each period become small in comparison with its average value. In the distributed amplification case [Fig. 2(b)], similar behavior occurs, except that jitter starts to grow from $L = 0$ and has overall smaller values.

In the next two sections, we calculate timing jitter accounting for local gain variations which occur invariably in real DM systems. In Section IV, we consider the case in which gain is provided by erbium ions distributed throughout the fiber link and take into account pump absorption and depletion $[g(z) \neq \alpha]$ for the bidirectional pumping scheme. In Section V, we focus on the case of Raman amplification.

IV. Erbium-Based Distributed Amplification

To calculate the actual variations of the gain $g(z)$ along the fiber, we use the two-level model of [15]. We solve numerically the multiple rate equations, accounting for gain saturation and pump depletion and assuming a bidirectional pumping scheme at 1480 nm. The inversion factor $n_{\rm sp}$ is obtained using

$$n_{\rm sp} = \sigma_e N_2/(\sigma_e N_2 - \sigma_a N_1) \tag{26}$$

where N_2 and N_1 are the ion densities of the upper and lower energy levels participating in stimulated emission, respectively, and σ_e and σ_a are the emission and absorption cross sections for the signal wavelength, respectively. The distributed gain can be written as $g(z) = \Gamma(\sigma_e N_2 - \sigma_a N_1)$, where Γ is the overlap factor between the doped region and the fiber mode. Neglecting the population N_3 of the third and higher levels, the total dopant density is $N_t = N_1 + N_2$. The parameter $n_{\rm sp}$ is then related to the gain as

$$n_{\rm sp} = \frac{\sigma_e}{\sigma_e + \sigma_a}\left[1 + \frac{\sigma_a \Gamma N_t}{g(z)}\right]. \tag{27}$$

We take $\sigma_e = 3.9 \times 10^{-21}$ cm^2, $\sigma_e = 3.5 \times 10^{-21}$ cm^2 and $\Gamma = 0.4$, the values appropriate for a Ge–Er-doped silica fiber at 1550 nm [16]. From the noise standpoint of view, N_t should be as small as possible. However, pump power increases as N_t is approaches its minimum possible value [7], [17]. As a compromise, we choose $N_t = 5.5 \times 10^{14}$ cm^{-3}, a value that requires pump power of about 100 mW for a 80-km pump-station spacing. We also consider a larger density value of $N_t = 9 \times 10^{14}$ cm^{-3} with a reduced pump power of about 50 mW. Such values are normally used for distributed erbium-doped fibers [7]. For each density value, we calculate timing jitter numerically using (12) with the actual gain profile and using (16) obtained for ideal loss compensation $[g(z) = \alpha]$. In both cases, inversion parameter $n_{\rm sp}$ is calculated from (26). For perfect loss compensation $n_{\rm sp}$ is constant with values of 1.4 and 1.97 for the N_t values given above.

Fig. 3 shows the timing jitter calculated at the end of each amplifier. Solid curves represent timing jitter with the actual gain profile and dotted curves represent timing jitter assuming $g = \alpha$. Timing jitter for the case of lumped amplification with $n_{\rm sp} = 1.5$ is also shown for comparison (dashed curve). The input parameters in each case are calculated by solving the variational equations numerically and are close to the parameters used in Section III. In order to verify, how much the soliton interaction itself would limit the transmission distance, the three cases shown in Fig. 3 were checked for propagation of a 40-Gb/s pseudorandom pulse train by solving (1) numerically with the split-step method. As an example, we solve (1) using $u(0, t) = \sum b_n u_n(0, t)$, where b_n is a binary random variable with values 0 and 1, and $u_n(0, t)$ is given by (11). In the case of distributed amplification with $N_t = 5.5 \times 10^{14}$ cm^{-3}, using $T_0 = 4.48$ ps, $C = -1.0$, and $E_0 = 0.0593$ pJ (parameters, corresponding to 3.11-ps minimum pulsewidth, accounting for the actual gain profile), we obtain the contour map shown in Fig. 4. These results were obtained without including amplifier noise and show that interaction among solitons does not affect

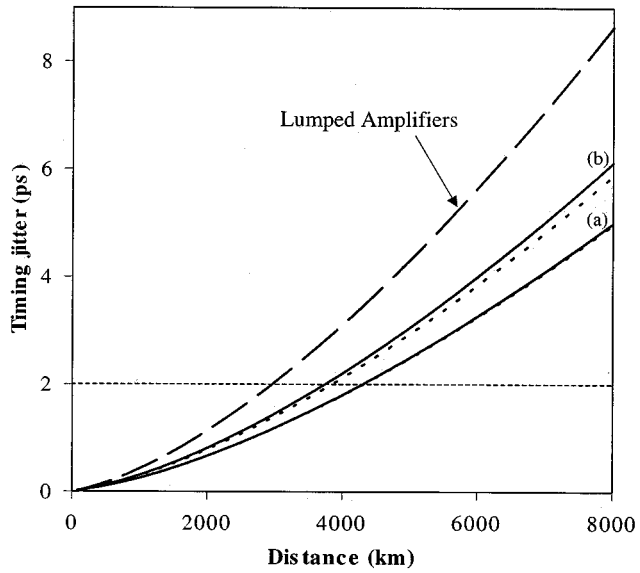

Fig. 3. Timing jitter at the end of each map period for the systems with erbium-based amplification (solid lines) for the dopant densities of (a) $N_t = 5.5 \times 10^{14}$ cm^{-3} and (b) $N_t = 9 \times 10^{14}$ cm^{-3}. Dotted lines show the results obtained assuming perfect loss compensation. Dashed line represents timing jitter for the same DM system with lumped amplification.

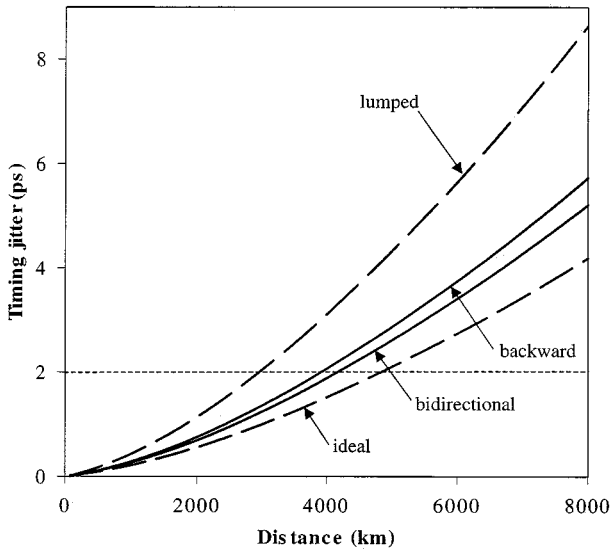

Fig. 5. Timing jitter at the end of each map period for distributed Raman amplification (solid lines) with bidirectional and backward pumping schemes. For the same DM system, lumped amplification ($n_{\rm sp} = 1.5$) and ideal distributed amplification ($n_{\rm sp} = 1$) are also shown for comparison (dashed lines).

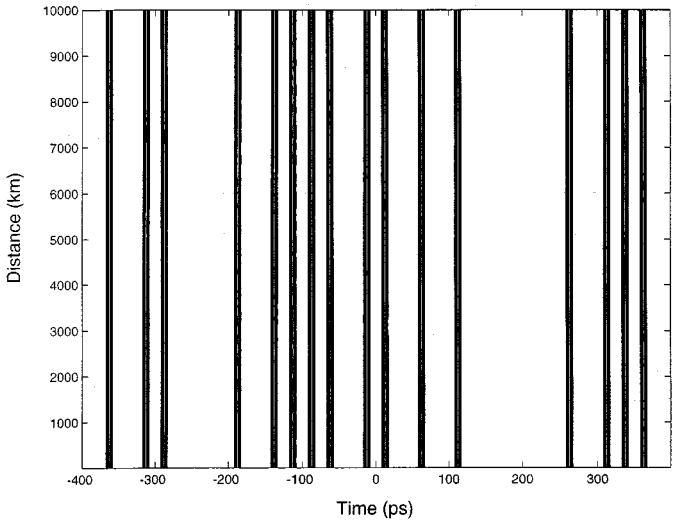

Fig. 4. Contour map of the bit sequence over 10 000 km for the 40-Gb/s system employing erbium-based distributed amplification with bidirectional pumping.

the pulse train at distances as large as 10 000 km. The results for the other two cases from Fig. 3 look similarly.

Fig. 3 shows that it is possible to achieve about 40% jitter reduction using distributed amplification with bidirectional pumping. Assuming Gaussian statistics for timing jitter σ, the bit-error rate (BER) can be found as

$$\mathrm{BER} = \frac{2}{\sqrt{2\pi}\sigma}\int_{T_{\rm B}/2}^{\infty} \exp\left(-\frac{t^2}{2\sigma^2}\right) dt = \mathrm{erfc}\left(\frac{T_{\rm B}}{2\sqrt{2}\sigma}\right) \approx \frac{4\sigma}{\sqrt{2\pi}T_{\rm B}} \exp\left(-\frac{T_{\rm B}^2}{8\sigma^2}\right) \tag{28}$$

where $T_{\rm B}$ is the bit slot and $\mathrm{erfc}(x) \equiv (2/\sqrt{\pi})\int_x^{\infty} \exp(-y^2)\, dy$. According to (28), for a BER of less than 10^{-9}, timing jitter should be less than 8% of the bit slot [2]. This value can be increased to 12% by using a forward error correction technique that can tolerate a BER of 10^{-4}. In the following discussion, we use the 8% criteria, which gives a value of 2 ps for the limiting timing jitter at 40 Gb/s. The dashed line in Fig. 3 shows that transmission distance is limited to about 2900 km in the case of lumped amplification, but can be increased up to 4300 km using the distributed amplification scheme. The dotted lines in Fig. 3 show that timing jitter is well approximated by the analytical result in (16), especially for relatively low dopant concentration values. The reason for better agreement for lower N_t values is that gain variations become smaller as N_t is reduced. Note that even for larger values of N_t, (16) is accurate to within a few percent.

V. Raman Distributed Amplification

In this section, we consider the distributed Raman amplification (DRA) scheme for the same dispersion map used earlier. The input parameters, corresponding to the 3.11-ps minimum pulsewidth, are $T_0 = 4.737$ ps, $C = -1.1$, and $E_0 = 0.0494$ pJ for Raman amplification with bidirectional pumping, and $T_0 = 4.696$ ps, $C = -1.08$, and $E_0 = 0.192$ pJ for backward pumping. These parameters were obtained by solving the variational equations [9] and were checked numerically for the 40-Gb/s propagation over long distance. For both pumping schemes, we use $n_{\rm sp} = [1 - \exp(-h\nu/kT)]^{-1} \approx 1.13$ at room temperature. Gain variations $g(z)$ for Raman amplification are calculated analytically using the condition of full loss compensation and neglecting pump depletion [9].

Fig. 5 shows timing jitter at the end of each amplifier as a function of transmission distance for bidirectional and backward pumping schemes. The limiting cases of lumped and ideal distributed amplification are shown for comparison. Considerable reduction occurs for both bidirectional and backward pumping schemes, although the bidirectional pumping

scheme gives smaller jitter values. The horizontal dashed line in Fig. 4 shows that transmission distance can be increased up to about 4200 km using a bidirectional Raman amplification scheme, whereas it would be limited to 2900 km for lumped amplifiers. Larger jitter values for a backward pumping scheme result from larger gain variations along the fiber. According to (12), timing jitter is proportional to $n_{\rm sp}$ and is inversely proportional to the input energy of the pulse. Although the $n_{\rm sp}$ parameter for Raman amplification is almost the same as for ideal distributed amplification, timing jitter is larger for Raman amplification. This is the consequence of larger gain variations along the fiber when Raman amplification is used. Comparing Figs. 3 and 4, we note that jitter values are within 10% of each other for Raman and erbium-based distributed amplification, although gain variations are larger in the Raman case. This is due to larger $n_{\rm sp}$ values for erbium dopants.

We consider now the practical case of hybrid amplification, in which a coded pulse train is amplified periodically using a module consisting of a lumped fiber amplifier and a Raman-pump laser injected backward into the fiber to provide the DRA. In this hybrid scheme, total fiber losses $G_{\rm tot}$ are compensated using the combination of lumped and Raman amplification such that $G_R + G_L = G_{\rm tot}$, or, equivalently

$$\exp\left(\int_0^{L_A} g_R(z)\,dz\right) + G_L = \exp\left(\int_0^{L_A} \alpha(z)\,dz\right) \quad (29)$$

where g_R and G_R are, respectively, local and accumulated Raman gain, G_L is the gain of lumped amplifier, and L_A is the amplifier spacing. The same dispersion map is used and input parameters are also comparable to those given earlier. Fig. 6 shows timing jitter after each amplifier as a function of transmission distance for several values of the Raman gain. While the smallest value of jitter occurs when 100% of losses are compensated using DRA, considerable reduction occurs even when losses are only partially compensated by the Raman gain.

We consider the question whether distributed amplification can allow a longer amplifier spacing. Fig. 7 shows timing jitter after 3100 km as a function of the Raman gain for 40-Gb/s systems employing a hybrid amplification scheme with amplifier spacings of 60, 80, and 100 km. The systems have six, eight, and ten map periods within each amplifier spacing, respectively, while the other parameters are the same as before. In each case, jitter is reduced by up to 40% by using DRA. More importantly, the use of lumped amplifiers alone leads to limiting jitter in excess of 2 ps when L_A exceeds 70 km. In contrast, amplifiers can be placed as much as 100 km apart when an hybrid amplification scheme is employed. The required Raman gain is only 2 dB for 80-km spacing but becomes 10 dB when amplifiers are 100 km apart.

Finally, we investigate timing jitter dependence on the map strength of the system. To change the map strength, we vary the values of the second-order dispersion β_{21} and β_{22} while keeping the average dispersion $\bar{\beta}_2$ and minimum pulsewidth $T_{\rm min}$ constant. Fig. 8(a) shows timing jitter dependence on the map strength at a distance of 4000 km for systems with lumped

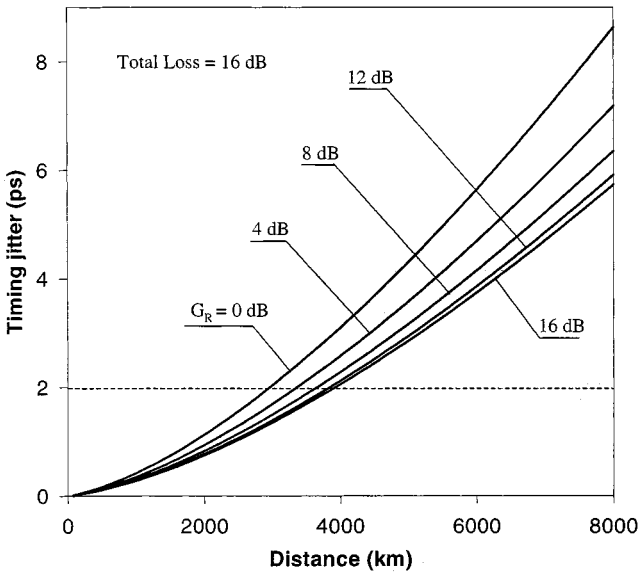

Fig. 6. Timing jitter after each amplifier as a function of transmission distance for several values of Raman gain. Losses are 16 dB over 80 km of amplifier spacing.

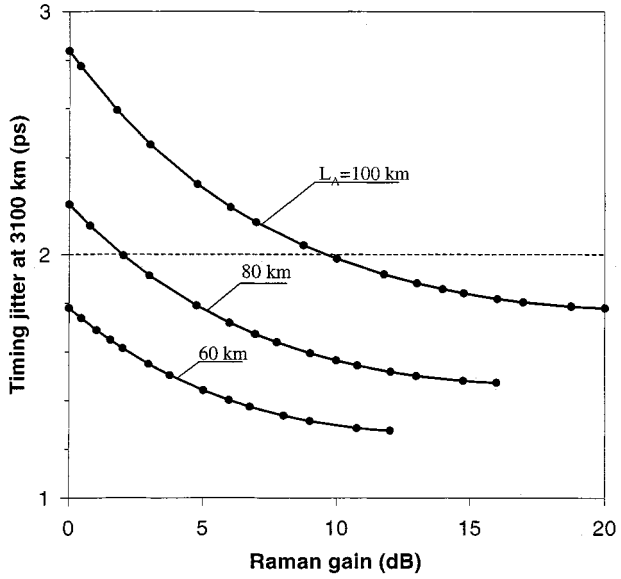

Fig. 7. Timing jitter after 3100 km as a function of Raman gain for amplifier spacings of 60, 80, and 100 km.

amplifiers and bidirectionally pumped DRAs. The $n_{\rm sp}$ parameter values used are the same as in Fig. 5. Solid curves correspond to $T_{\rm min} = 3.11$ ps and are suitable for a 40-Gb/s system, while dashed curves with $T_{\rm min} = 8$ ps are appropriate for a 10–15 Gb/s system. In each case, timing jitter decreases as map strength is increased. The reason for this decrease is that larger values of the map strength require higher values of input pulse energy in order to keep the pulsewidth fixed. Since timing jitter is inversely proportional to the pulse energy, the jitter decreases as map strength increases. Input pulse energies for each value of the map strength are shown on Fig. 8(b) and support this conclusion. Note, however, that pulse breathing increases significantly for large map strengths, and the system may be limited by soliton interaction.

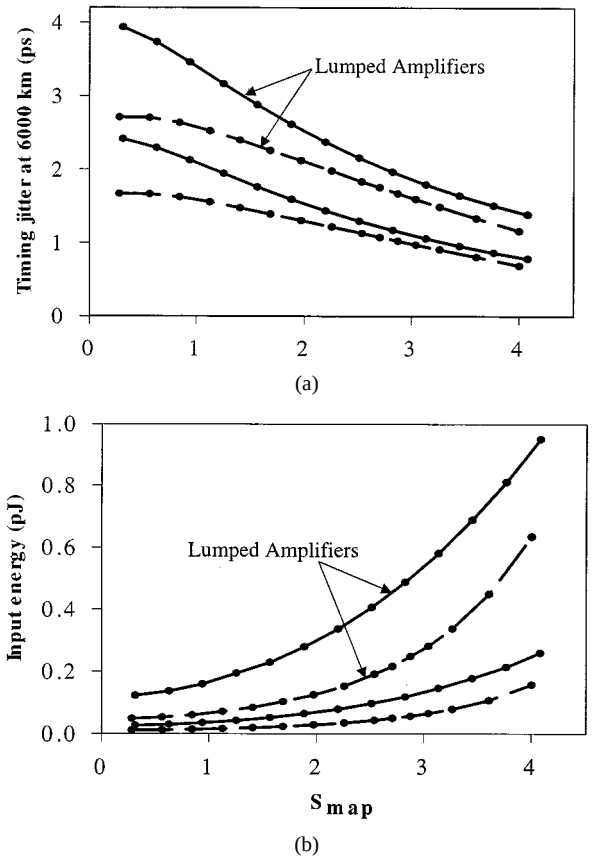

Fig. 8. (a) Timing jitter after 4000 km as a function of the map strength in DM systems with lumped and bidirectionally pumped Raman amplification. Minimum pulsewidth remains fixed at 3.11 ps (solid lines) and at 8 ps (dashed lines). (b) Corresponding input energy values.

Fig. 8(a) also shows that timing jitter values are larger for shorter pulsewidths, although shorter pulsewidths require larger pulse energies. We have verified that this behavior holds for erbium distributed amplification as well. The reason for this can be understood from (16) and (22), which show that the term growing as z^3 with distance z is proportional to the ratio $(1 + C_0^2)/(T_0^2 E_0)$. Numerical solutions of the variational equations show that this ratio increases for smaller T_0 values, thus giving rise to a larger timing jitter.

VI. Conclusion

We have compared the ASE-induced timing jitter in dispersion-managed systems for the cases of lumped, distributed, and hybrid Raman amplification schemes. We show that, while the erbium-based distributed amplification gives the smallest timing jitter value, considerable reduction occurs when bidirectional, backward, or even partial Raman amplification is employed. We have derived an analytical expression for the timing jitter at any position within the fiber link in the case of ideal distributed amplification for which losses are exactly compensated by gain at every point. We show that in the case of a low erbium-dopant density, timing jitter is well approximated by this formula. We also derive an analytical expression for the timing jitter for lumped amplifiers and compare it to the case of distributed amplification. Finally, we show that timing jitter decreases for stronger maps at a given bit rate (fixed minimum pulsewidth).

Acknowledgment

The authors thank Dr. D. Chowdhury of Corning and Dr. S. N. Volkov of University of Rochester for helpful discussions.

References

[1] J. P. Gordon and H. A. Haus, "Random walk of coherently amplified solitons in optical fiber transmission," *Opt. Lett.*, vol. 11, no. 10, pp. 665–667, 1986.
[2] D. Marcuse, "An alternative derivation of the Gordon–Haus Effect," *J. Lightwave Technol.*, vol. 10, pp. 273–278, Feb. 1992.
[3] V. S. Grigoryan, C. R. Menyuk, and R.-M. Mu, "Calculation of timing and amplitude jitter in dispersion-managed optical fiber communications using linearization," *J. Lightwave Technol.*, vol. 17, pp. 1347–1356, Aug. 1999.
[4] S. Kumar and F. Lederer, "Gordon–Haus effect in dispersion-managed soliton systems," *Opt. Lett.*, vol. 22, no. 24, pp. 1870–1873, 1997.
[5] R.-M. Mu, V. S. Grigoryan, C. R. Menyuk, E. A. Golovchenko, and A. N. Pilipetskii, "Timing-jitter reduction in a dispersion-managed soliton system," *Opt. Lett.*, vol. 23, no. 12, pp. 930–932, 1998.
[6] B. A. Malomed, F. Matera, and M. Settembre, "Performance of optically amplified dispersion-compensated links: Reduction of the time jitter for return to zero signals," *Opt. Commun.*, vol. 143, pp. 193–198, 1997.
[7] K. Rottwitt, J. H. Povlsen, and A. Bjarklev, "Long distance transmission through distributed Erbium-doped fibers," *J. Lightwave Technol.*, vol. 11, pp. 2105–2112, Dec. 1993.
[8] K. Rottwitt, A. Bjarklev, J. H. Povlsen, O. Lumholt, and T. P. Rasmuseen, "Fundamental design of a distributed Erbium-doped fiber amplifier for long-distance transmission," *J. Lightwave Technol.*, vol. 10, pp. 1544–1552, Nov. 1992.
[9] G. P. Agrawal, *Applications of Nonlinear Fiber Optics*. New York: Academic, 2001, ch. 7, 8.
[10] H. A. Haus, "Quantum noise in a solitonlike repeater system," *J. Opt. Soc. Amer. B*, vol. 8, no. 5, pp. 1122–1126, 1991.
[11] S. N. Vlasov, V. A. Petrishchev, and V. I. Talanov, "Averaged description of wave beams in linear and nonlinear media," *Radiophys. Quantum Electron.*, vol. 14, p. 1353, 1971.
[12] S. K. Turitsyn, M. F. Fedoruk, E. G. Shapiro, V. K. Mezentsev, and E. G. Turitsyna, "Novel approaches to numerical modeling of periodic dispersion-managed fiber communicaion systems," *IEEE J. Select. Topics Quantum Electron.*, vol. 6, pp. 263–275, Mar./Apr. 2000.
[13] T. I. Lakoba and D. J. Kaup, "Shape of stationary pulse in strong dispersion management regime," *Electron. Lett.*, vol. 34, no. 11, pp. 1124–1125, 1998.
[14] V. S. Grigoryan, T. Yu, E. A. Golovchenko, C. R. Menyuk, and A. N. Pilipetski, "Dispersion-managed soliton dynamics," *Opt. Lett.*, vol. 22, no. 21, pp. 1609–1611, 1997.
[15] P. C. Becker, N. A. Olsson, and J. R. Simpson, *Erbium-Doped Fiber Amplifiers*. New York: Academic, 1999, pp. 144–157, 204.
[16] W. L. Barnes, R. I. Laming, E. J. Tarbox, and P. R. Morkel, "Absorption and emission cross section of Er^{3+} doped silica fibers," *IEEE J. Quantum Electron.*, vol. 27, pp. 1004–1010, Apr. 1991.
[17] K. Rottwitt, J. H. Povlsen, A. Bjarklev, O. Lumholt, B. Pedersen, and T. Rasmuseen, "Noise in distributed Erbium-doped fibers," *IEEE Photon. Technol. Lett.*, vol. 5, pp. 218–219, Feb. 1993.

Ekaterina Poutrina (S'02), photograph and biography not available at time of publication.

Govind P. Agrawal (M'83–SM'86–F'96), photograph and biography not available at time of publication.